Ion Acoustic Waves Observed at Comet 67P/Churyumov-Gerasimenko

H. Gunell[1], H. Nilsson[2], M. Hamrin[3], A. Eriksson[4], R. Maggiolo[1], P. Henri[5], K. Altwegg[6], C.-Y. Tzou[6], M. Rubin[6], K.-H. Glaßmeier[7], G. Stenberg Wieser[2], C. Simon Wedlund[8], J. De Keyser[1], F. Dhooghe[1], G. Cessateur[1], and A. Gibbons[1,9]

[1]Royal Belgian Institute for Space Aeronomy [2]Swedish Institute of Space Physics, Kiruna [3]Umeå University, Sweden [4]Swedish Institute of Space Physics, Uppsala

[5]Université d'Orléans, France [6]University of Bern, Switzerland [7]Technical University of Braunschweig, Germany, [8]University of Oslo, Norway, [9]Université Libre de Bruxelles, Belgium

<herbert.gunell@physics.org>

Abstract

Some of the neutral water molecules that are emitted from the nucleus are ionised, and these new ions are accelerated by an electric field, forming a thin beam that is observed with instruments on the spacecraft. When the neutral density is high, ions are scattered by these neutrals to cause heating of the ion distribution. We observe ion acoustic waves in data from the Langmuir probe, and these waves are weakly damped when the bulk ion distribution is cold. But when a warm ion distribution is present, the waves are heavily damped to levels below the threshold for detection.

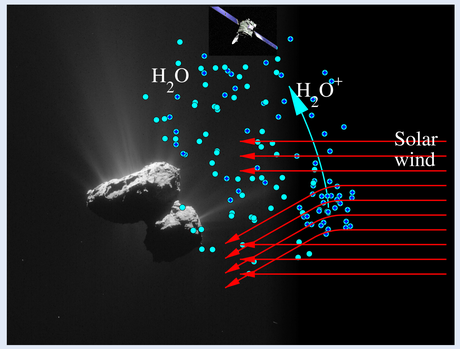

Illustration of particle motion at 67P, showing the beginning of the H_2O^+ trajectories and deflection of solar wind ions [1, 2, 3, 4]. Photo of nucleus and spacecraft: ESA.

Rosetta data

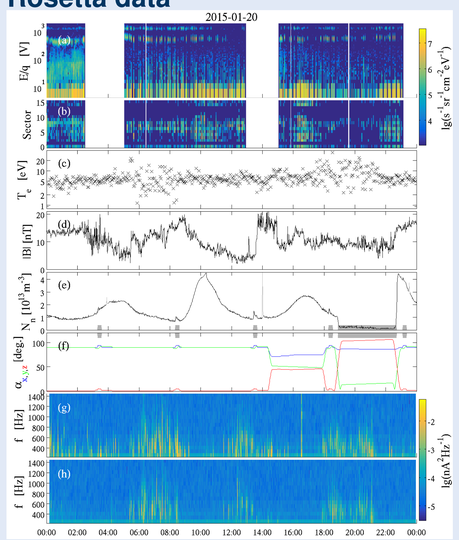

Figure 1:
a) Ion energy spectrum measured by RPC-ICA. The colour coded quantity is the differential particle flux summed over all viewing directions. The energy scale has been adjusted for V_e and V_{offset}. **b)** Differential particle flux of hot water ions ($9\,\text{eV} \lesssim E \lesssim 23\,\text{eV}$ when E is adjusted for offset and spacecraft potential) for the different sectors of the RPC-ICA instrument. **c)** Electron temperature observed by RPC-LAP. **d)** Magnitude of the magnetic flux density B seen by RPC-MAG. **e)** Neutral gas density measured by ROSINA-COPS. **f)** Angles between the coordinate axes of the spacecraft frame of reference and the direction to the nucleus of the comet. **g)** Power Spectral density of the current to Langmuir probe 1 in the frequency range $200\,\text{Hz} < f \leq 1450\,\text{Hz}$. **h)** Power Spectral density of the current to Langmuir probe 2 for $200\,\text{Hz} < f \leq 1450\,\text{Hz}$.

Distribution functions

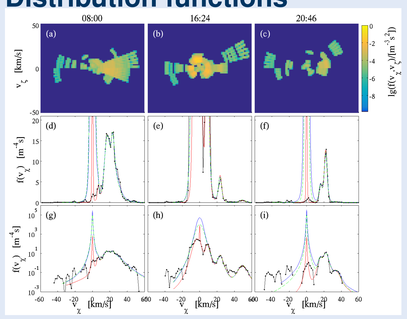

Figure 2:
Water ion distribution functions observed at 08:00 (left column), 16:24 (mid column), and 20:46 (right column) on 20 January 2015. Panels **a–c)** show the two-dimensional projection of the distribution function on a plane in velocity space. Panels **d–f)** show the one-dimensional projection of the distribution functions on the horizontal axis of panels **a–c)**. Panels **g–i)** show the same one-dimensional projection on a logarithmic vertical scale. The black curves show the data. The red, blue, and green curves show three different functions used as fits to the data. Corrections for the instrument offset and spacecraft potential have been applied. Densities and temperatures for the model curves are shown in Table 1.

Table 1: Parameters of the H_2O^+ distributions shown in Fig. 2 and the plasma parameters used to calculate the dispersion relations in Fig. 5. T_e is the electron temperature; T_{ci} is the temperature of the cold ion population and n_e is the plasma density.

	red curve			green curve			blue curve		
time	n_e	$k_B T_e$	$k_B T_{ci}$	n_e	$k_B T_e$	$k_B T_{ci}$	n_e	$k_B T_e$	$k_B T_{ci}$
	[10^6m^{-3}]	[eV]	[eV]	[10^6m^{-3}]	[eV]	[eV]	[10^6m^{-3}]	[eV]	[eV]
08:00	0.7	7	0.0086	83	10.2	0.0163	165	7	0.0086
16:24	7.35	7	0.011	67	7.9	1.26	266	7	0.81
20:46	0.4	7	0.0090	69	12.9	0.0090	210	7	0.0090

Langmuir probe spectra

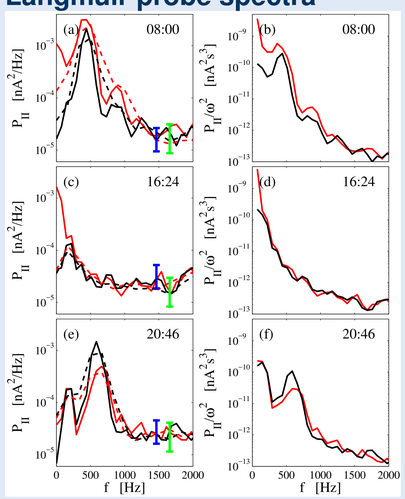

Figure 3:
Panels **a)**, **c)**, and **e)** show power spectral densities of the currents to the Langmuir probes at 08:00, 16:24, and 20:46 on 20 January 2015. The red lines show probe 1 and the black lines probe 2. The dashed lines show lower frequency resolution, where data points taken while the RPC-MIP instrument was running have been removed. The error bars show the 95 % confidence intervals for the solid curves in blue and the dashed curves in green. Panels **b)**, **d)**, and **f)** show power spectral densities divided by ω^2.

Dispersion relations

A distribution function can be written as a sum of several components each described by a "simple pole expansion" of the form [5, 6]

$$f(v) = M(v)T(v),$$
$$M(v) = \left[1 + \frac{(v - v_{\text{d}0})^2}{2v_{\text{t}}^2} + \ldots + \frac{1}{m!}\left(\frac{(v - v_{\text{d}0})^2}{2v_{\text{t}}^2}\right)^m\right]^{-1} \quad (1)$$
$$T(v) = \left[1 + \left(\frac{v - v_{\text{d}1}}{v_{\text{c}}}\right)^{2n}\right]^{-1},$$

Functions of the form described by Eq. (1) can be written as a sum involving simple poles and residues in the complex phase velocity plane:

$$f(v) = \sum_j \frac{a_j}{v - b_j} \quad (2)$$

In a plasma composed of different species the dielectric function is [e.g. 7]

$$\epsilon(k,\omega) = 1 + \sum_\alpha \frac{\omega_{\text{p}\alpha}^2}{k^2} \int \frac{k \mathrm{d}f_\alpha(u)/\mathrm{d}u}{\omega - ku} du. \quad (3)$$

We integrate in the complex plane, closing the integral path in the upper half plane, and find the dispersion relations by solving [8]

$$\epsilon(k,\omega) = 1 - 2\pi i \sum_\alpha \omega_{\text{p}\alpha}^2 \sum_{b_{j,\alpha} \in U} \frac{a_{j,\alpha}}{(\omega - k b_{j,\alpha})^2} = 0 \quad (4)$$

Solar wind insignificance

Waves caused by the solar wind ions interacting with the cometary populations are heavily damped.

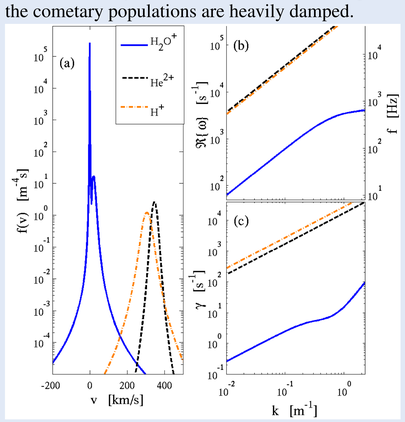

Figure 4:
Dispersion relations at 08:00 on 20 January 2015. **a)** Distribution functions for cometary water ions (solid blue curve) and solar wind protons (dash-dotted orange curve) and alpha particles (dashed black curve). **b)** Real part of ω as a function of wave number. **c)** The imaginary part of ω as a function of wave number. In this case $\gamma > 0$ for all three curves, which means that these modes are damped. The blue curves represent the same mode as the blue curves in Fig. 5.

Ion acoustic waves

We have computed dispersion relations for the distributions observed at the three times 08:00, 16:24, and 20:46 shown in Fig. 2. For each time three different functions, shown by the red, green, and blue curves, have been used to fit the data. The red curve represents a density estimated from direct integration of ion data; the green curve makes use of the density estimated by the Langmuir probe, and the blue curve represents a distribution with a somewhat higher density. The parameters are summarised in Table 1. The blue curves agree the best with the Langmuir probe spectra in Fig. 3.

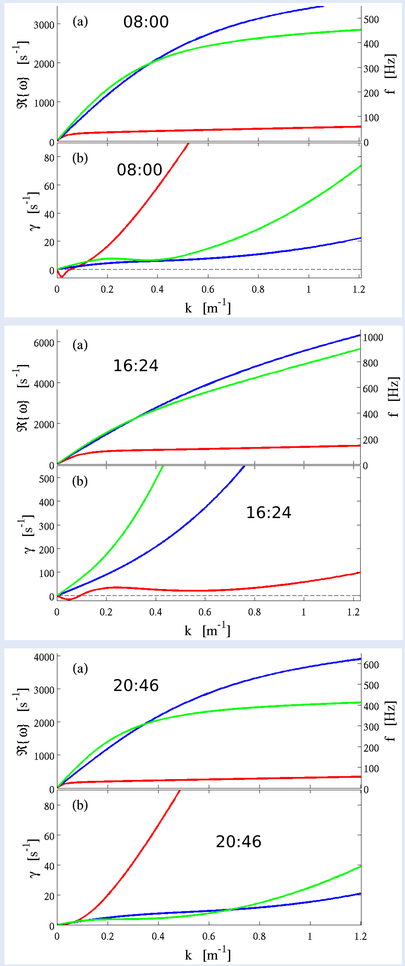

Figure 5:
Dispersion relations at 08:00, 16:24 and 20:46 on 20 January 2015. **a)** Real part of ω as a function of wave number. **b)** The imaginary part of ω as a function of wave number. For growing modes $\gamma < 0$ and for damped modes $\gamma > 0$. The red, blue, and green curves correspond to the distribution functions shown in Fig. 2d and g by the red, blue, and green curves, respectively.

Conclusions

We analysed data from instruments on board the Rosetta spacecraft.

- We have observed ion distribution functions with the RPC-ICA instrument [9]; ion acoustic waves and electron densities and temperature with RPC-LAP [10]. The densities are in good agreement with those obtained by RPC-MIP [11]. The neutral density is measured by ROSINA-COPS [12] and the magnetic field by RPC-MAG [13].
- Water ions dominate the ion time scale waves. Protons and alpha particles are not important.
- Ion acoustic waves, associated with the H_2O^+ ions are weakly damped,
- except at times when there is a warm (1 eV) isotropic ion population. At these times the ion acoustic waves are heavily damped.
- Although we do not measure the current in the plasma, it is not unlikely that the waves are generated by a current driven instability [14, 15, 16].
- The ion heating occurs as ions accelerated by a large scale electric field are scattered in velocity space by collisions with neutrals.

Acknowledgements

This work was supported by the Belgian Science Policy Office through the Solar-Terrestrial Centre of Excellence and by PRODEX/ROSETTA/ROSINA PEA 4000107705.

References

[1] H. Nilsson et al., *Science*, 347(6220), 2015.

[2] H. Nilsson et al., *Astronomy & Astrophysics*, 583:A20, 2015.

[3] E. Behar et al., *Geophys. Res. Lett.*, 43:1411–1418, 2016.

[4] E. Behar et al., *Astronomy & Astrophysics*, 596:A42, 2016.

[5] T. Löfgren and H. Gunell. *Physics of Plasmas*, 4:3469–3476, 1997.

[6] H. Gunell and F. Skiff. *Physics of Plasmas*, 8:3550–3557, 2001.

[7] N. A. Krall and A. W. Trivelpiece. *Principles of Plasma Physics*. McGraw-Hill, New York, 1973.

[8] H. Gunell and F. Skiff. *Physics of Plasmas*, 9:2585–2592, 2002.

[9] H. Nilsson et al., *Space Science Reviews*, 128:671–695, 2007.

[10] A. I. Eriksson et al., *Space Science Reviews*, 128(1):729–744, 2007.

[11] J. G. Trotignon et al., *Space Science Reviews*, 128(1):713–728, 2007.

[12] H. Balsiger et al., *Space Science Reviews*, 128:745–801, 2007.

[13] K.-H. Glassmeier et al., *Space Science Reviews*, 128:649–670, 2007.

[14] T. E. Stringer. *Journal of Nuclear Energy*, 6:267–279, 1964.

[15] N. Sato et al., *Physics of Fluids*, 19:70–73, 1976.

[16] P. Michelsen et al., *Plasma Physics*, 21:61–73, 1979.